CAN PERMAFROST SOIL THAW BE CHARACTERIZED BY HYPERSPECTRAL REFLECTANCE AND PLANT COMMUNITY STRUCTURE?

By

ANTHONY JOHN JUNQUEIRA GARNELLO

A Thesis Submitted to The Honors College

In Partial Fulfillment of the Bachelors degree
With Honors in

Ecology and Evolutionary Biology

THE UNIVERSITY OF ARIZONA

MAY 2015

Approved by:

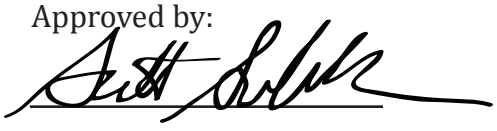

Dr. Scott Saleska
Department of Ecology and Evolutionary Biology

Can Permafrost Soil Thaw be Characterized by Hyperspectral Reflectance and Plant Community Structure?

Abstract

I investigated (1) whether stages of permafrost thaw were consistently associated with plant community composition and other land surface characteristics; (2) whether those different land surface characteristics could be consistently distinguished with remote sensing tools in a sub-arctic mire. I utilized plant area cover and topography to identify five distinct site-types as being characteristic of different stages of permafrost thaw, and 50 one square-meter plots were measured for species-specific area cover and pole-based hyperspectral reflectance. A Tukey-HSD comparison test showed that plant functional group richness decreased with permafrost thaw, and could readily be used to differentiate between stages of thaw. A discrete, stepwise canonical classification function with bootstrap cross validation showed a mean classification error rate of 7.3% +/- 7.3% (6.8%-9.65% 95% Confidence Interval). These results showed successful ground-truthing methods for regional-scale landscape classification, allowing for high temporal and spatial resolution of circumpolar permafrost thaw monitoring.

Introduction

Perennially frozen belowground soil layers (permafrost) are unique features of polar latitudes. In the Northern Hemisphere, permafrost regions occupy roughly 23% of exposed land area, and permafrost layers have been labeled as an Essential Climate Variable by the Arctic Climate Impact Assessment: on a global scale, permafrost soils play three key roles in Earth's climate system: (1) a geoindicator of environmental change at certain depths, (2) a direct line for transferring atmospheric temperature changes to Earth's hydrosphere, cryosphere, and biosphere, and (3) a feed-back contributor to climate change through the release of greenhouse gases such as methane and carbon dioxide accompanying thawing (Bäckstrand *et al.,* 2009; International Arctic Science Committee 2010). Climate models show warming trends for much of the arctic, leading to a widespread loss of permafrost soil area cover, and the potential release of belowground arctic soil carbon, estimated to contain 50% of global below-ground soil carbon (Tarnocai *et al.,* 2009; Callaghan *et al.,* 2010; Slater & Lawrence 2013; McCalley *et al.,* 2014). Soil active layer growth accompanies vegetative, topographical, and hydrological shifts in sub-arctic wetland systems, offering opportunities for the characterization of these surface-level consequences permafrost thaw (Schuur *et al.,* 2008).

Greenhouse gas fluxes from soil active layers depend on the extent of permafrost thawing, and the surface characteristics of thaw extent can be classified into discrete stages (Malmer & Wallen, 1996; Malmer *et al.,* 2005). These stages are characterized by specific plant species diversity and microtopography, but extensive research on the inter-site variation has not been done. Increased knowledge of the ecosystem dynamics that occur along a gradient of permafrost thawing can be useful in predicting future arctic system responses to climate change.

Traditional field methods of sampling plant composition are the ground level of accurately characterizing wetland thaw gradients, but are not plausible on a larger scale. Employment of remote sensing techniques will provide a scale-able, non-destructive way of monitoring these types of landscape consequences of permafrost thaw, but first require ground truthing methodology (Fitzgerald & Riordan, 2003).

High-resolution hyperspectral reflectance spectroscopy is sensitive to many plant cellular and soil properties (Thenkabail *et al.,* 2011). Using a pole-based field spectroradiometer to measure surface-level characteristics of permafrost thaw will provide basis for more widespread applications, and up-scaling techniques. Global scale analysis with hyperspectral reflectance methods are possible through satellites such as EO-1 Hyperion. With these global scale techniques, circumpolar mapping of arctic wetland landscapes will become possible, allowing for a greater understanding of the rate of permafrost-thaw-caused ecosystem transitioning. Additionally, carbon flux data linked with stages of permafrost thaw can be combined with global mapping to approximate global arctic soil-atmospheric carbon fluxes.

The goal of this project was to establish discrete characteristics of the surface consequences of permafrost soil thawing through the utilization of vegetation composition. Furthermore, the methodology of pole-based hyperspectral reflectance measurements aimed to provide ground-truthed measurements which will allow for scaling up these monitoring techniques. Recruiting higher spatial scale remote sensing technology can provide a real-time mapping of arctic landscape evolution. Also, when coupled with regional-scale carbon flux data, remotely-sensed landscape maps will yield a highly informative picture of the fate of terrestrial carbon with the changing arctic climate.

Materials and Methods

Location of study site

The study site is Stordalen Mire, located 10 km south of Abisko, Sweden, 68°22' N, 19°03'E. Stordalen Mire is a sub-arctic ombrotrophic fen located in the discontinuous permafrost region of northern Sweden, and is comprised of dwarf birch forests, elevated palsa hummocks, and thermokarst thaw-ponds. This study took place in July 2014, the middle of the summer growing season, which runs from snowmelt in May through August. This region experienced a mean annual temperature of 0.8°C, with a growing season (May 20th-Sept 1st) average temperature of 11.4°C for 2014 (Abisko Scientific Research Station, 2014).

Permafrost thaw gradient classification

The natural landscape progression that resulted from permafrost thaw was broken into five distinct categories based on dominant flora and apparent wetness **(Figure 1)**. Each stage had distinct floral and wetness features **(Table 1)**. The transition between stage III and IV are distinct because the water cycle moves from nutrient-poor ombrotrophic (precipitation-fed), to nutrient-rich minerotrophic (stream-fed).

Figure 1) Schematic cross section of surface and hydrologic effects of permafrost thawing, resulting in the five categories: Tall Shrub (I), Hummock (II), Semi-Wet (III), Wet (IV), and Tall Graminoid (V)–Figure adapted from Johansson, et al. 2006.

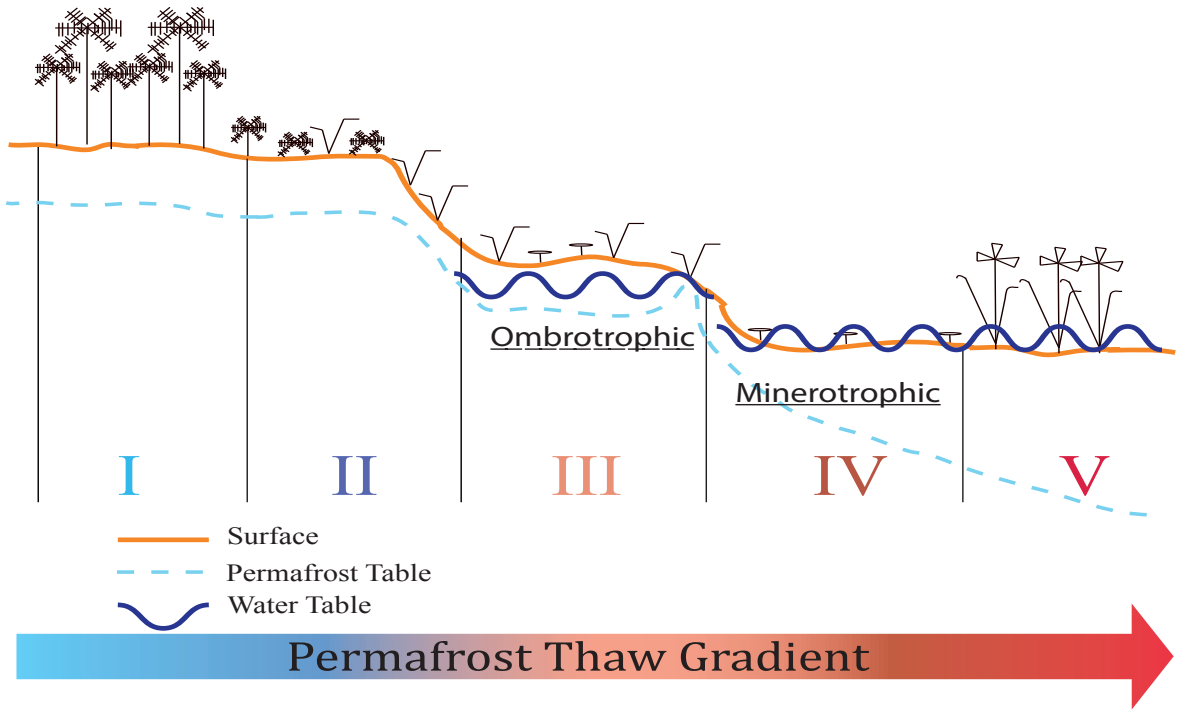

Table 1) Site Type Classifications and Characterizing Features

Site Type	**Characteristic Wetness, Plant Species,**
Tall Shrub (I)	Dry. *Cornus canadensis, Salix lopponum, Betula nana*
Hummock (II)	Dry. *Eriophorum vaginatum, Empetrum hermaphroditum.* Lichens
Semi-Wet (III)	Ombrotrophic. *Sphagnum* spp, *Andromeda polifolia, E. vaginatum*
Wet (IV)	Minerotrophic. Open water dominated
Tall Graminoid (V)	Minerotrophic. Open water. *E. angustofolium, C. rostrata*

GPS Mapping of Stordalen Mire

High resolution GPS coordinates were recorded along the boardwalk at Stordalen Mire (GeoExplorer® 6000 Series GeoXT Handheld, Trimble inc). Using GIS software, 500 random coordinate points were generated inside a 15m buffer zone along the Mire boardwalk. Of these 500 points, 50 were utilized as measured experimental plots.

Vegetation Composition

Each coordinate selected from the buffer zone was centered in a meter square plot, and classified into one of five site types: tall shrub, hummock, semi-wet, wet, tall graminoid, according to vegetation composition and apparent wetness **(Table 1)**. Ten plots were measured according to each site type, accounting for 50 plots in total. At each site, plant species composition and species percent area cover was measured using a square meter quadrant with 64 sub-quadrants, plant identifications aided by local botanical specialists and previously published literature (Johansson *et al.,* 2006; Johansson *et al.,* 2011).

Hyperspectral Collection

Reflectance values from 350nm to 2500nm were captured at each plot*(One semi-wet plot was not measured before experiment end) using a pole-based hyperspectral spectroradiometer (ASDinc FieldSpec Pro 4). The sampling interval was 1.4 nm at 350-1050 nm, and 2nm at 1000-2500nm, with a 100 millisecond scanning time. Due to instrument limitations, the entire $1m^2$ plot could not be captured into one spectra directly, therefore, a new procedure was created: Each plot was divided into $0.25m^2$ sub-plots, and a minimum of three spectra collected for each sub-plot, of each plot. The optical cable of the spectroradiometer was fastened to a pole at 1.15 m aboveground, fastened with angular perpendicularity to the ground surface. This optical cable height allowed for the capture of $0.25m^2$ per-spectra, according to the designed 25° field of view of the fore optic **(Figure 2).** Each spectrum was collected with the fore optic positioned nadir to the center of each sub-plot. Final spectral data for each plot was obtained through averaging together each of the sub-plot spectra. Spectra were collected through July 2014, between 11am and 1:30pm on cloudless days. The instrument underwent optimization and referencing to a calibration block (Spectralon, Labsphere, North Sutton, NH) before measuring each plot, minimizing the change of light conditions between reference and spectra collection.

Figure 2: Pole-Based Spectral Collection Methodology

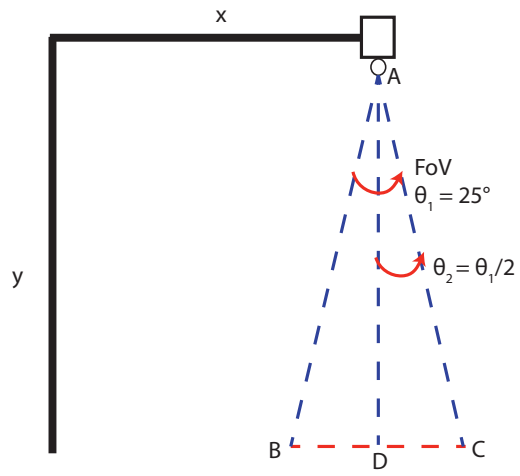

The manufactured Field of View (FoV) of the fore optic was 25° (θ). In order to capture 0.25m^2 of plot area in the spectra (BD, BD=DC), the height from the ground (AD), must be calculated using geometry:

$$AD = DC/\tan(\theta/2)$$

$$AD = 0.25m/\tan(12.5°)$$

$$AD = 1.13m$$

The final pole instrument was built with a height (y) of 1.15m, and a bridge (x) length of 0.75m.

Data Quality Control

Collected reflectance values underwent data quality control: eliminating the spectral regions between 1350nm: 1450nm, 1811nm: 1940nm, and 2400nm: 2500nm, corresponding to low signal-to-noise ratios in regions reflected by atmospheric water (Ryerson, 1998) and instrument insensitivities. Plots that had spectral regions with values outside ± 1.96 standard deviations of the site mean were eliminated from hummock, semi-wet, wet, and tall graminoid site types, resulting in the elimination of one spectra from the hummock, wet, and tall graminoid site-types. The site-type tall shrub had four plots excluded due to an improper methodology: Spectra were collected under shady trees, with highly varying sun/light conditions from wind. The final data set was reduced from 50 plots to 42, comprised of 6 tall shrub, and 9 plots for hummock, semi-wet, wet, and tall graminoid site-types.

Statistical Analyses

A forward, stepwise, discrete canonical analysis (DA) was employed to determine whether site type could be remotely sensed at the ground level using high fidelity spectroscopy. Canonical analysis works to explain the differences between these site types by extracting

underlying gradients of variation (through variable reduction) among the spectra, while maximizing the variation between sites and minimizing the variation within sites (McGarigal *et al.,* 2000). Variable reduction was a necessary step for building predictive models with the spectral data, where approximately 1800 wavelengths are available for use as model predictor variables. A bootstrapping procedure was employed to test the power of DA in classifying plot site-type: The data was partitioned into training and validating sets (67%, 33%, respectively), then stepwise variable selection iteratively added 10 wavelengths (selected according to lowest p-value) into the model, stopping after each variable addition to record the model results. This overall procedure was repeated 100 times, each trial with a randomly generated partitioning of the data into training and validating bins.

Plant Functional Diversity

Species percent cover data from each plot were binned into plant functional groups according to Chapin, *et al.* (1996) **(Figure 3)**. Values for functional group presence were averaged among plots to obtain an average plant functional group percent composition of each site type **(Table 2)**.

Figure 3) Plant Functional Group Distribution

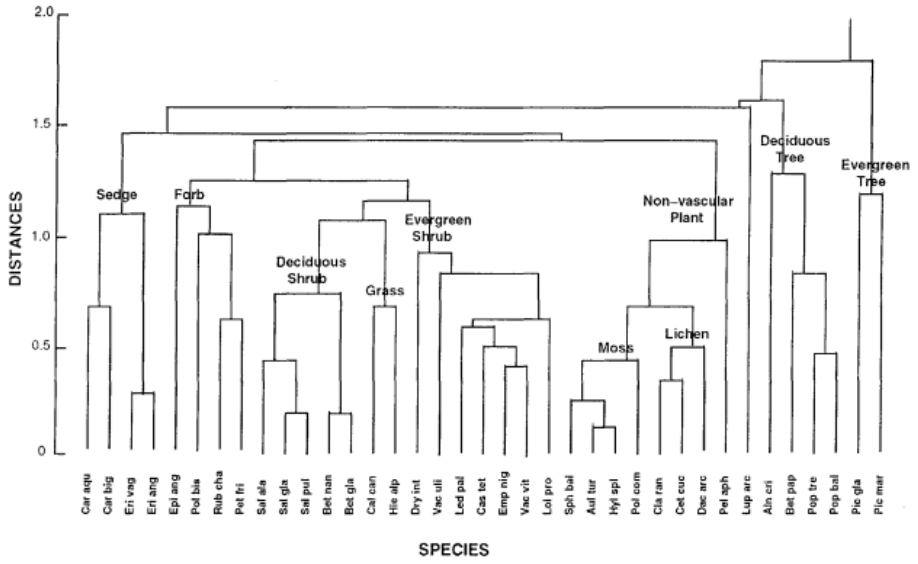

Fig. 2. Dendrogram showing the similarity among major tundra plant species and boreal trees and their groupings into functional types, based on Euclidean distance and average-linkage method. Species are: Aln cri *Alnus crispa,* Aul tur *Aulacomnium turgidum*, Bet gla *Betula glandulosa*, Bet nan *B. nana*, Bet pap *B. papyrifera*, Cal can *Calamogrostis canadensis*, Car aqu *Carex aquatilis*, Car big *C. bigelowii*, Cas tet *Cassiope tretragona*, Cet cuc *Cetraria cucullata*, Cla ran *Cladonia rangiferina*, Dac arc *Dactylina arctica,* Dry int *Dryas integrifolia*, Emp nig *Empetrum nigrum* ssp. *hermaphroditum*, Epi ang *Epilobium angustifolium*, Eri ang *Eriophorum angustifolium*, Eri vag *E. vaginatum* ssp. *spissum*, Hie alp *Hierochloë alpina*, Hyl spl *Hylocomium splendens*, Led pal *Ledum palustre* ssp. *decumbens*, Loi pro *Loiseleuria procumbens*, Lup arc *Lupinus arcticus*, Pel aph *Peltigera aphthosa*, Pet fri *Petasites frigidus*, Pic gla *Picea glauca*, Pic mar *P. mariana*, Pol bis *Polygonum bistorta* ssp. *plumosum*, Pol com *Polytrichum commune*, Pop bal *Populus balsamifera*, Pop tre *P. tremuloides*, Rub cha *Rubus chamaemorus*, Sal ala *Salix alaxensis*, Sal gla *S. glauca*, Sal pul *S. pulchra*, Sph bal *Sphagnum balticum*, Vac uli *Vaccinium uliginosum*, Vac vit *V. vitis-idaea*.

Adapted from Chapin *et al.,* 1996

Results

Plant Community Composition

Functional group diversity decreased along the thaw gradient: with the near-complete elimination of the forbs, deciduous shrubs, and evergreen shrubs from the semi-wet, wet, and tall graminoid site types **(Table 2)**. The proportion of three plant functional groups (forbs, deciduous shrubs, and evergreen shrubs), were found to be significantly lower in semi-wet, wet, and tall graminoid plots when compared to tall shrub and hummock plots. This supports the utilization of techniques that rely on the surface vegetation composition to monitor or characterize landscape evolution.

Table 2) Site Type Percent Composition of Plant Functional Groups

Site Type	Evergreen Shrub*	Deciduous shrubs*	Sedges	Forbs*	Sphagnum moss	Deciduous trees	Richness
Tall Shrub (I)	0.28	0.28	0.10	0.26	0.07	0.01	6
Hummock (II)	0.42	0.10	0.29	0.14	0.05	0.00	5
Semi-Wet (III)	0.00	0.00	0.49	0.00	0.51	0.00	2
Wet (IV)	0.00	0.01	0.76	0.00	0.23	0.00	3
Tall Graminoid (V)	0.00	0.00	0.85	0.00	0.15	0.00	2

*Represent functional groups that are statistically different *comparing Hummock/Tall Shrub with Semi-Wet, Wet, and Tall Graminoid) (Significance based on Tukeys HSD ANOVA)

Hyperspectral Analysis

Plotting the average site-type spectra ± the standard error shows confidence in applying statistical inference methods to hyperspectral reflectance data **(Figure 4).**

Figure 4a) Site Type Average Reflectance Signatures with Standard Errors

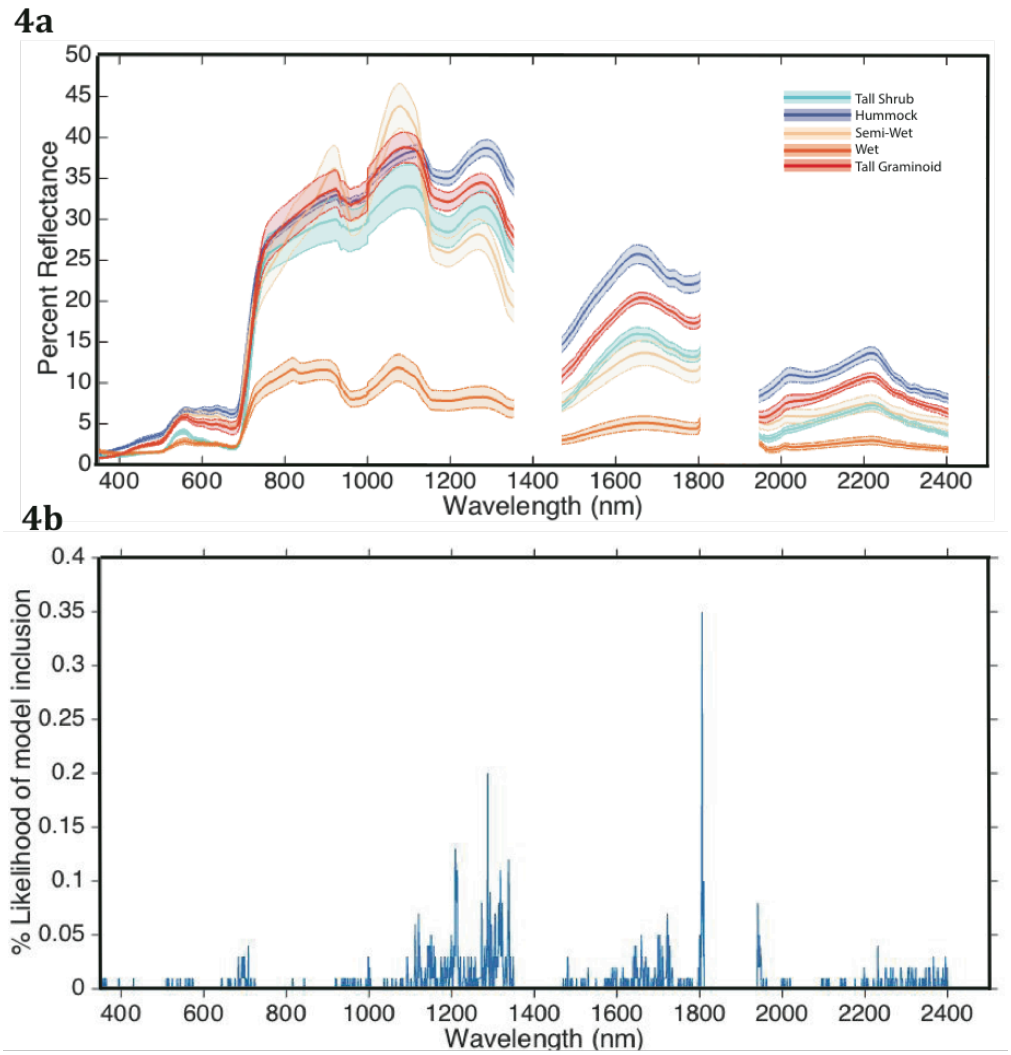

Figure 4b) Bootstrap Model Wavelength Inclusion Likelihood

Figure 4a: Site Type average reflectance ± standard error. **Figure 4b**: the proportion of wavelengths included in each of the bootstrap model iterations (n=100).

Spectral regions after 1200nm appear to distinguish site-types. The shaded regions represent the site average spectra ± the standard error: Standard Error = Standard Deviation / square root (sample size). The relative likelihood of wavelength inclusion in the model trends with spectral regions that distinguish the site types, suggesting a relative importance of certain wavelengths in readily differentiating thaw stage.

The bootstrapping method with 100 iterations of the stepwise DA model showed a minimal standard error in classification rate when including four wavelengths, with a mean misclassification rate of 8.2% (± 7.3%), and a 95% confidence interval of 6.8%-9.65% **(Figure 5, Table 3)**. With the validation sample size equal to 14 plots, 7.1% misclassification amounts to 1 out of 14 plots classified incorrectly.

Figure 5) Distribution of Classification Error from Model Bootstrapping

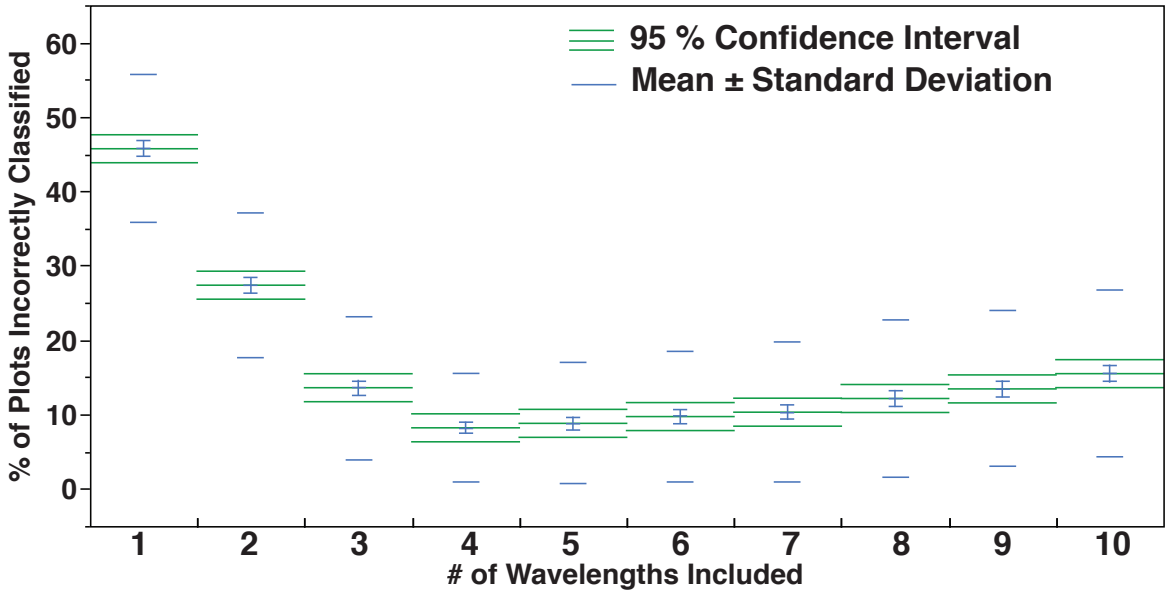

Table 3) Table of Statistics for Figure 5

	Classification Error Percent			95% Confidence Interval	
Number of Wavelengths	**Mean**	**Std Dev**	**Std Error of Mean**	**Lower**	**Upper**
1	45.71	9.97	0.99	43.73	47.69
2	27.37	9.78	0.97	25.43	29.31
3	13.59	9.64	0.96	11.67	15.50
4	8.2	7.28	0.73	6.76	9.64
5	8.8	8.09	0.81	7.20	10.41
6	9.71	8.73	0.87	8.00	11.44
7	10.3	9.46	0.95	8.42	12.18
8	12.14	10.55	1.06	0.05	14.23
9	13.43	10.48	1.05	11.36	15.51
10	15.48	11.18	1.12	13.26	17.70

The lowest **Mean** value of data misclassification results from the inclusion of four wavelengths, as well as the minimal standard error and confidence intervals. This suggests the optimal number of canonical variables to use before model over fitting is four, though the consequences of model over fitting are minimal through the inclusion five wavelengths.

With each DA model iteration, a Canonical Plot was created as a visual representation of plot classification. Each Canonical Variable is the result of a linear multivariate combination of the reflectance values corresponding to the wavelengths selected. The Canonical Variables are the axis upon which each site type is defined, and each data point plotted.

Figure 6) Example Discriminant Canonical Classification Plot

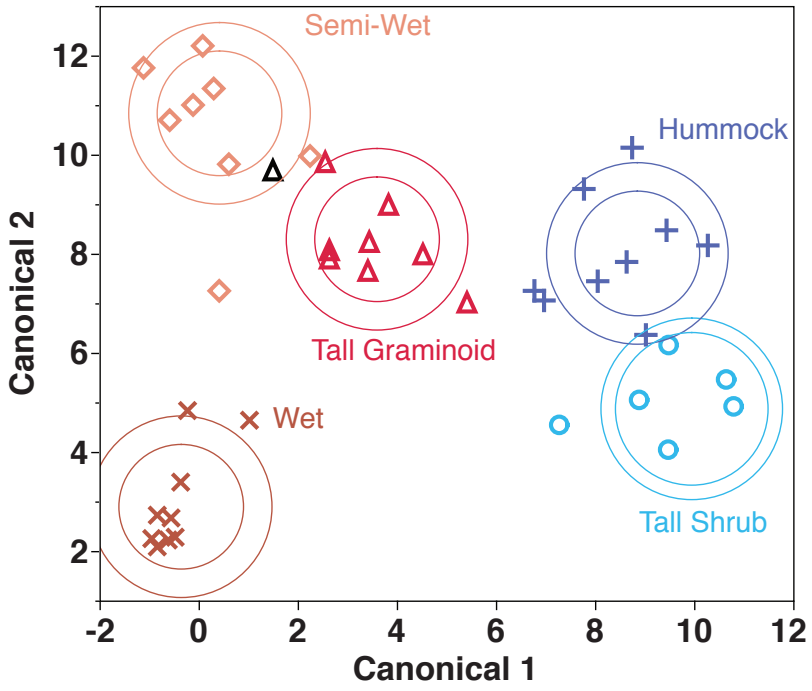

This is an example 2D canonical graph. 28 plots were used to train this model, and an independent 14 plots used in validation. 13/14 plots were correctly classified with $p < 0.01$, except for the highlighted point (misclassified a Tall Graminoid as a Semi-Wet). This figure has four canonical dimensions, corresponding to linear combinations of the reflectance from the wavelengths 1211, 1213, 1320, and 1804 nm.

Discussion

Because the nature of remote sensing is dependent on surface characteristics, this study focused partly on the changing plant composition along the gradient of permafrost thaw.

Plant composition consequences of permafrost thaw

The dominant plant functional groups of sedges and sphagnum mosses are strong indicators of the extent of permafrost thaw **(Table 2)**. This result agrees with previous work done in classifying plant composition in arctic wetlands (Malmer & Wallen, 1996;

Malmer *et al.,* 2005), reinforcing the inference that plant community compositions are strong indicators of landscape evolution due to permafrost thawing. It is expected that through the drastic loss of functional group diversity, there will be a definite shift in ecosystem dynamics: including alterations to carbon and water cycling from the elevated soil aeration brought about by a higher density of sedge species, as shown in McCalley *et al.* (2014) and Johansson *et al.,* (2006). This work shows that plant functional groupings correlate well with stage of permafrost thaw. More analyses are required to detail the expected ecological responses of dominant sedge and moss functional groups.

Hyperspectral reflectance analysis of permafrost thaw

Canonical analysis is an effective approach at characterizing the surface-level characteristics along this permafrost thaw gradient, with dominant spectral signals existing between 1000nm-1400nm, 1450nm-1810nm, and 1900nm-2400nm **(Figure 4)**. These spectral regions are known to correlate strongly with plant-cell mesophyll, water content, and soil water content (Ryerson, 1998). Small signals appear near the red-edge and early near infrared spectral zones, suggesting that the application of a multi-band camera to differentiate site type will yield a less robust classifying ability. This result agrees with the work done by Bubier *et al.,* (1997), reinforcing the inference that different plant functional groups (sphagnum mosses, vascular plants, lichens) have different spectral signatures. However, because this study utilized a larger spatial scale than Bubier *et al.* (1997) ($10cm^2$), I have shown that the spectral signatures of different plant functional groups are not only resolvable on larger scales, but also remain distinct through up-scaling landscape classification methodology. Additionally, this work provides the first high-resolution ground truthing methodology for landscape classification at Stordalen Mire. Previous work done in mapping Stordalen Mire has relied on pixel-differentiation from aerial photos, introducing sources of error in interpretation (Johansson *et al.,* 2006).

What is left to be done includes comparing these hyperspectral signatures to other sub-arctic wetlands across the globe. Due to the commonality of circumpolar floral functional groups (Chapin *et al.* 1996), it is likely that these hyperspectral signatures will be present in other longitudes. Furthermore, future remote sensing studies of the arctic are expected to increase in occurrence because of the strong potential climate change impacts of thawing permafrost soils. The trajectory of remote sensing studies is in enhancing our large-scale collection techniques, but satellite and aerial methods typically require high-resolution ground truthing. High landscape heterogeneity in these regions complicate low-resolution landscape classification schemes, particularly in the task of linking surface changes over time to soil-atmosphere carbon cycling, where unseen error in landscape classification will directly lead to error in climate change modeling.

Conclusion

I showed a successful methodology for characterizing surface consequences of permafrost thaw, these methods include 1) characterizing vegetation functional groups along different stages of thaw, and 2) applying hyperspectral reflectance techniques in a discrete, canonical model to classify plots along different stages of thaw. These hyperspectral techniques provide ground-truthing methodology for further experimentation with up scaling. Scaling up will yield much more time and cost effective means of monitoring this landscape change over time, enabling the addition of a temporal scale to future arctic wetland remote sensing studies.

References

Abisko Scientific Research Station. (2014). *Temperature data 2014.* Available from Abisko Sceintific Research Station Web site: http://www.polar.se

Bokhorst, S. F., Bjerke, J. W., Tømmervik, H., Callaghan, T. V. & Phoenix, G. K. Winter warming events damage sub-Arctic vegetation: consistent evidence from an experimental manipulation and a natural event. *J. Ecol*. **97**, 1408–1415(2009).

Bubier, J. L., Rock, B. N. & Crill, P. M. Spectral reflectance measurements of boreal wetland ecosystems at small spatial scales exhibit distinctly different. *J. Geophys. Res.* **102,** 29,483–29,494 (1997).

Callaghan, T. V. et al. (2010). A new climate era in the sub-Arctic: Accelerating climate changes and multiple impacts. *Geophys. Res. Let.* **37** (14).

Chapin, F. S., Bret-Harte, M. S., Hobbie, S. E. & Zhong, H. Plant functional types as predictors of transient responses of arctic vegetation to global change. *J. Veg. Sci.* **7**, 347–358 (1996).

International Arctic Science Committee, (2010). Arctic Climate Impact Assessment (full report). Retrieved from http://www.eoearth.org/view/article/150186

Fitzgerald, D. & Riordan, B. Permafrost and Ponds. Remote sensing and GIS used to monitor Alaska wetlands at the landscape level. Agroborealis **35,** 30–37 (2003).

Johansson, T. et al. Decadal vegetation changes in a northern peatland, greenhouse gas fluxes and net radiative forcing. *Glob. Chang. Biol.* **12**, 2352–2369 (2006).

Johansson, M. et al. Past and Present Permafrost Temperatures in the Abisko Area: Redrilling of Boreholes. *Ambio.* **40**, 558–565 (2011).

Malmer, N. & Wallen, B. Peat Formation and Mass Balance in Subarctic Ombrotrophic Peatland around Abisko , Northern Scandinavia. *Ecol. Bull*. 79–92 (1996).

Malmer, N., Johansson, T., Olsrud, M. & Christensen, T. R. Vegetation, climatic changes and net carbon sequestration in a North-Scandinavian subarctic mire over 30 years. *Glob. Chang. Biol.* (2005).

McCalley, C. K. et al. Methane dynamics regulated by microbial community response to permafrost thaw. *Nature* **514,** 478–481 (2014).

Ryerson, R. (1998). Manual of remote sensing (3rd ed.) (A. Rencz, Ed.). New York, New York: J. Wiley.

Schuur, E. a. G. et al. Vulnerability of Permafrost Carbon to Climate Change: Implications for the Global Carbon Cycle. *Biosc.* **58**, 701 (2008).

Slater, A. G. & Lawrence, D. M. Diagnosing present and future permafrost from climate models*. J. Clim.* **26**, 5608–5623 (2013).

Tarnocai, C. et al. Soil organic carbon pools in the northern circumpolar permafrost region. *Glob. Biogeochem. Cycles.* **23** (2009).

Thenkabail, P., Lyon, J., & Huete, A. (2012). Hyperspectral remote sensing of vegetation. Boca Raton, Florida: CRC Press.